INTERNATIONAL JOURNAL FOR NUMERICAL METHODS IN FLUIDS, VOL. 23, 691–710 (1996)

THE SIMULATION OF SOME MODEL VISCOELASTIC EXTENSIONAL FLOWS

S. GUNTER, P. TOWNSEND AND M. F. WEBSTER

Institute of Non-Newtonian Fluid Mechanics, University of Wales, Swansea, Singleton Park, Swansea SA2 8PP, UK

SUMMARY

The numerical simulation of three model viscoelastic extensional flows is considered: sink flow, model draw-down and conical section draw-down. A transient finite element scheme with a pressure correction method is employed to analyse the numerical treatment of such problems for Oldroyd-B and Phan-Thien/Tanner constitutive models. Both decoupled and coupled formulations are compared for these highly convective flows and effective mechanisms are proposed for removing numerical oscillations in the temporally developing solution. In pure viscoelastic extensional flow from an initial stress-free state, the maximum stress level attained decreases with increase in material relaxation time. When this is followed by stress relaxation, as in conical section draw-down, increasing the relaxation time inhibits stress decay.

KEY WORDS: viscoelastic; extensional flow; wirecoating; Taylor–Galerkin; finite elements; pressure-correction

INTRODUCTION

This study is concerned with the numerical simulation of complex, highly viscoelastic flows that arise in the coating with an appropriate polymer of wires and fibre-optic cables. There are two common die designs employed in such coating processes: pressure tooling extrusion and tube extrusion. The principal distinction in action between these two coating processes is that in pressure tooling, used for narrow-bore wires, the moving wire is coated with polymer whilst still resident in the die geometry, whereas in tube extrusion, relevant for wide-bore cables, coating of the moving cable takes place outside the confines of the die, invoking a draw-down flow. Tube extrusion combines the processes of tube tooling and conical section draw-down.

Both situations lead to a highly extensional component of flow due to both the dragging action of the wire or cable and the converging annular flow in the die. Large normal stresses may result as a consequence. In the present context we are interested primarily in analysing the extensional flows that result in tube extrusion (see Figure 1) and constructing model problems that render the numerical solution tractable in such demanding circumstances.

The numerical simulation of pressure tooling flow for viscous materials has received attention in the works of Caswell and Tanner,[1] Wagner and Mitsoulis,[2] Mitsoulis,[3] Pittman and Rashid[4] and Mitsoulis *et al.*[5] These works concentrated on shear flow in both isothermal and non-isothermal prevailing conditions. A study highlighting the problems involved in viscous modelling of

CCC 0271–2091/96/070691–20

Received September 1995
Revised January 1996

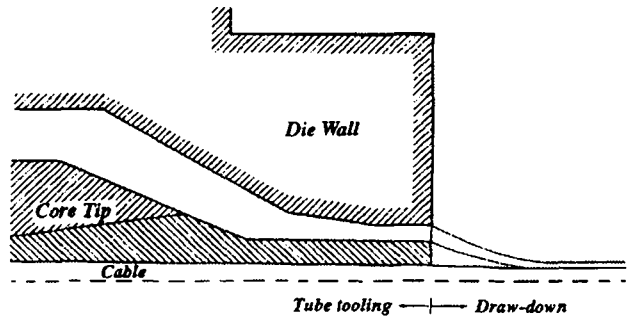

Figure 1. Schematic illustration of tubing extrusion geometry

extensional effects in wirecoating flows has been reported by Blythe *et al.*[6] It was concluded that to successfully model wirecoating flows, a viscoelastic modelling approach is required. This is certainly true if the principal interest is the stress distribution in the polymer coating.

The polymers of interest are polyethylenes of low, medium and high density.[7,8] They are highly viscoelastic and possess the properties of both extension-thinning and shear-thinning viscosities. These materials have been characterized by appropriate rheological measurements[7] and we endeavour to fit their material properties to non-linear viscoelastic constitutive equations from the class of Phan-Thien/Tanner models.[9] Such models are expressed in terms of implicit differential equations for the fluid stress components with a dependence on fluid memory as well as viscosity.

The flows of immediate interest are predominantly extensional flows which may be approximated by two-dimensional convection-dominated problems under an axisymmetric frame of reference. Such flows demand sophisticated numerical methods in their solution treatment. Here we employ a transient finite element method of a Taylor–Galkerin/pressure correction form that has the additional embedded features of consistent streamline upwinding and a semi-implicit time-stepping procedure. This is a powerful technique employed elsewhere to provide solutions to highly viscoelastic flows[10,11] and one that is analysed here for its performance under convection-dominated circumstances.

PROBLEM SPECIFICATION

The coating of wide-bore cables requires the union of the two flow processes of tube tooling extrusion and draw-down (see Figure 1). The axis of the wire is an axis of symmetry so that flow takes place in a converging annular geometry. The molten polymer is injected into the tooling die and flows under the combined influences of a pressure gradient and drag flow induced by the wire. Flow in the converging section of the tooling geometry represents a combination of shear and extension: since the die walls are assumed to be non-slip surfaces, a shear flow is established; the reduction in cross-sectional area of the tooling geometry generates an increase in velocity in the flow direction (to maintain a constant flow rate) and hence causes some extension. This complex motion generates both normal and shear stresses in the molten polymer. The level of stress fixed in the final polymer coating may have an influence on the surface finish and durability of the cable coating. In an attempt to reduce this locked-in level of stress, an end section is appended to act as a stress-relaxing region, where the velocity field is allowed to reach a fully developed shear flow. This is important in viscoelastic flow, since stress decay is dependent on the relaxation time of the material and will not occur instantaneously upon cessation of strain, as would be the case for an inelastic fluid.

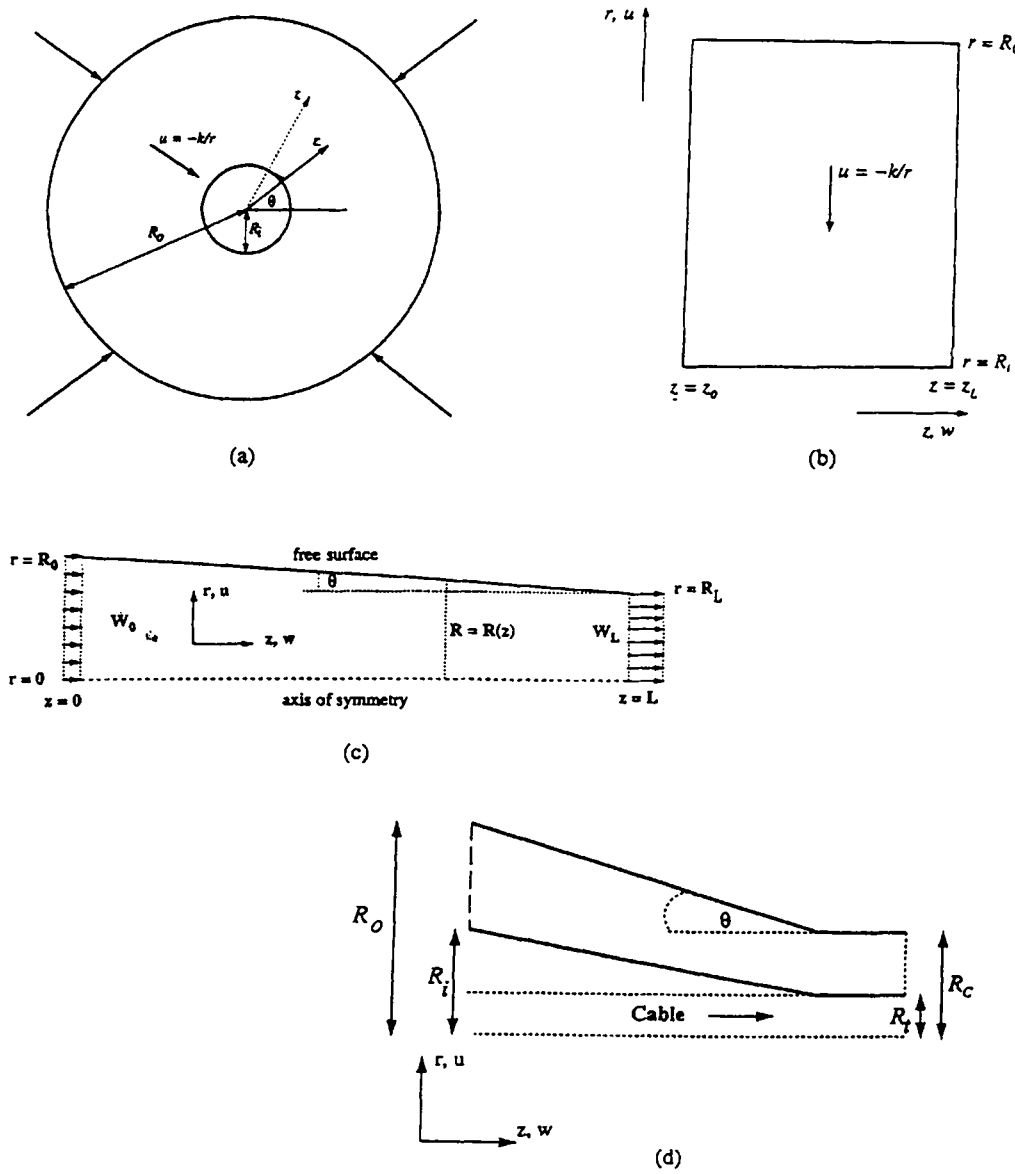

Figure 2. Schematic illustrations of (a) sink flow (perspective view), (b) two-dimensional sink flow, (c) model draw-down and (d) conical section draw-down geometries

As the fluid exits the tube tooling extrusion geometry, it enters the draw-down flow regime. The draw-down geometry (see Figure 2(d)) consists of an extension section where the fluid is again stressed, primarily in the direction of flow, owing to the pulling action of the cable. Since the fluid surfaces are traction-free, this is an axisymmetric flow dominated by extensional effects (shear contributions being minimal) in an outer section of the draw-down cone, formed by the revolution of the outer traction-free surface about the axis of symmetry. The stresses are allowed to relax as the fluid travels in contact with the cable in the coating section, where the final coating thickness is determined. The polymer is then subjected to rapid cooling to produce a finished product.

One vital consideration of the analysis of this combined process is the determination of viscoelastic stresses produced by the flow in these two regimes: how they grow and relax. Furthermore, open questions to be resolved include: which flow regime produces the greatest level of stress (where and why) and what modifications can be made to the geometry and flow properties to minimize the amount of 'locked-in' stress in the finished product?

In the extension region of the draw-down geometry and in the converging section of the tube tooling geometry the reduction in cross-sectional area gives rise to an increase in velocity in the flow direction and hence a growth in the normal stress. (For draw-down the increase in velocity and stress will depend on the draw-down ratio—the ratio of the cross-sectional area of flow at the exit of the tube tooling geometry to that at the final coating thickness.) In order to proceed with the study for the draw-down flow, we first turn to a much simpler model representation, that of radial sink flow, where pure extension of a viscoelastic fluid in one dimension may be analysed numerically. This permits the gradual consideration of each of the various complications present in one-dimensional extensional flow when solved in two dimensions. Sink flow provides us with an extremely useful model representation of the dominant flow behaviour of the full draw-down problem and extensional flow in the tube tooling geometry. It is open to a wide range of numerical tests and facilitates comparison against an analytic solution for Newtonian, Maxwell and Oldroyd-B fluid models. By solving this problem in two dimensions and freezing the kinematics, we can study the stress solution development under vanishing traction conditions or fixed stress on the free boundaries and monitor the temporal development of the solution.

We also analyse stress growth for viscoelastic flow in a model draw-down geometry, that of extensional flow in a conical geometry, made up of an inclined traction-free surface forming a conical volume of revolution about an axis of symmetry. This represents a slightly more complex flow problem than that of sink flow, with the radius of the cone varying in the axial direction introducing a degree of shear to the problem, making it two-dimensional. At the same time this provides a simplification of the conical section draw-down problem in that it removes the degree of freedom associated with the lower traction-free surface. The line of approach adopted is then as follows. By solving the sink flow problem, we seek to gain insight into the solution procedure and possible difficulties arising from the numerical solution of extension-dominated flows. This will then aid in the subsequent study of the model draw-down problem and ultimately for the conical section draw-down flow specification. The Weissenberg number is the ratio of the characteristic time of the fluid (a relaxation time) to a characteristic time of the process (typically the reciprocal of a characteristic strain rate) and can be expressed as $We = V\lambda/L$, where V is a characteristic velocity, L is a characteristic length and λ is the relaxation time of the fluid. Owing to the viscoelastic nature of the coating materials and the operating time scales ($\ll 1$ s), wirecoating processes take place at values of Weissenberg number much greater than unity—typically $O(10)$. To obtain a deeper understanding of viscoelastic flow at such levels of Weissenberg number, we solve these model problems up to $We = 30$ and report on the effects of increasing elasticity (fluid relaxation time).

GOVERNING EQUATIONS AND NUMERICAL METHOD

For an incompressible fluid the stress tensor $\boldsymbol{\sigma}$ may be written as

$$\boldsymbol{\sigma} = -p\boldsymbol{\delta} + \boldsymbol{\tau}, \tag{1}$$

where p is the isotropic pressure, $\boldsymbol{\delta}$ is the Kronecker delta and $\boldsymbol{\tau}$ is the extra-stress tensor.

We consider the extra-stress tensor to be made up of a polymeric solute component $\mathbf{T}$ and a viscous solvent component $2\mu_2\mathbf{D}$:

$$\boldsymbol{\tau} = \mathbf{T} + 2\mu_2\mathbf{D}. \tag{2}$$

The chosen constitutive model for the polymeric solvent component is a Phan-Thien/Tanner (PTT) model in its exponential form, which may be expressed as

$$\exp\left(\frac{\varepsilon\lambda}{\mu_1}\text{trace}[\mathbf{T}]\right)\mathbf{T} + \lambda\overset{\square}{\boldsymbol{T}} = 2\mu_1\mathbf{D}, \tag{3}$$

where

$$\overset{\square}{\boldsymbol{T}} = \left(1 - \frac{\xi}{2}\right)\overset{\triangledown}{\boldsymbol{T}} + \frac{\xi}{2}\overset{\triangle}{\boldsymbol{T}}$$

represents a linear combination of the upper $\overset{\triangledown}{\boldsymbol{T}}$, and lower, $\overset{\triangle}{\boldsymbol{T}}$, convected derivatives and $0 \leqslant \xi \leqslant 2$. $\overset{\square}{\boldsymbol{T}}$ may also be written as

$$\overset{\square}{\boldsymbol{T}} = \frac{\partial\mathbf{T}}{\partial t} + \mathbf{u}\cdot\nabla\mathbf{T} - \nabla\mathbf{u}\cdot\mathbf{T}(\nabla\mathbf{u}\cdot\mathbf{T})^{\dagger} + \xi[\mathbf{D}\cdot\mathbf{T} + (\mathbf{D}\cdot\mathbf{T})^{\dagger}].$$

For this model, λ is a relaxation time and μ_1 and μ_2 are the polymeric and solvent viscosities respectively. The parameter ε is related to control of the extensional behaviour and ξ controls the extent of the shear thinning.

We adopt dimensionless variables

$$\mathbf{x} = L\mathbf{x}', \qquad t = \frac{L}{V}t', \qquad \mathbf{u} = V\mathbf{u}', \qquad p = \frac{\mu_0 V}{L}p',$$

$$\boldsymbol{\tau} = \frac{\mu_0 V}{L}\boldsymbol{\tau}', \qquad \lambda = \frac{L}{V}\lambda', \qquad \mu_i = \mu_0\mu_i',$$

where V is a characteristic velocity, L is a characteristic length and μ_0 is the zero-shear viscosity ($\mu_0 = \mu_1 + \mu_2$).

The system of governing equations consists of conservation of mass and transport of momentum and stress, which may be expressed non-dimensionally as (discarding the prime notation for convenience of representation)

$$\nabla\cdot\mathbf{u} = 0, \tag{4}$$

$$Re\frac{\partial\mathbf{u}}{\partial t} = \nabla\cdot(2\mu_2\mathbf{D} + \mathbf{T}) - \nabla p - Re\mathbf{u}\cdot\nabla\mathbf{u} \tag{5}$$

and

$$We\frac{\partial\mathbf{T}}{\partial t} = 2\mu_1\mathbf{D} - \exp\left(\frac{\varepsilon We}{\mu_1}\text{trace}[\mathbf{T}]\right)\mathbf{T} - We\{u\cdot\nabla\mathbf{T} - \nabla\mathbf{u}\cdot\mathbf{T} - (\nabla\mathbf{u}\cdot\mathbf{T})^{\dagger} + \xi[\mathbf{D}\cdot\mathbf{T} + (\mathbf{D}\cdot\mathbf{T}^{\dagger}]\}, \tag{6}$$

respectively, where

$$Re = \frac{\rho VL}{\mu_0} \quad \text{and} \quad We = \frac{V}{L}\lambda$$

are the non-dimensional groups of Reynolds and Weissenberg numbers respectively, and ρ is the fluid density.

A semidiscrete representation of this system renders a time-stepping structure to the scheme and an operator-splitting approach that generates a number of fractional-staged equations over each time step interval $[t^n, t^{n+1}]$. With the definition

$$f = \exp\left(\frac{\varepsilon We}{\mu_1}\text{trace}[\mathbf{T}]\right),$$

this intermediate system takes the following form:

stage 1a

$$\frac{2Re}{\Delta t}(\mathbf{u}^{n+1/2} - \mathbf{u}^n) = [\nabla \cdot (\mathbf{T} + 2\mu_2\mathbf{D}) - Re\mathbf{u} \cdot \nabla u - \nabla p]^n + \nabla \cdot \mu_2(\mathbf{D}^{n+1/2} - \mathbf{D}^n),$$

$$\frac{2We}{\Delta t}(\mathbf{T}^{n+1/2} - \mathbf{T}^n) = (2\mu_1\mathbf{D} - f\mathbf{T})^n - We\{\mathbf{u} \cdot \nabla\mathbf{T} - \nabla\mathbf{u} \cdot \mathbf{T} - (\nabla\mathbf{u} \cdot \mathbf{T})^\dagger + \xi[\mathbf{D} \cdot \mathbf{T} + (\mathbf{D} \cdot \mathbf{T})^\dagger]\}^n;$$

stage 1b

$$\frac{Re}{\Delta t}(\mathbf{u}^* - \mathbf{u}^n) = (\nabla \cdot \mathbf{T} - Re\mathbf{u} \cdot \nabla\mathbf{u})^{n+1/2} + [\nabla \cdot (2\mu_2\mathbf{D}) - \nabla p]^n + \nabla \cdot \mu_2(\mathbf{D}^* - \mathbf{D}^n),$$

$$\frac{We}{\Delta t}(\mathbf{T}^{n+1} - \mathbf{T}^n) = (2\mu_1\mathbf{D} - f\mathbf{T})^{n+1/2} - We\{\mathbf{u} \cdot \nabla\mathbf{T} - \nabla\mathbf{u} \cdot \mathbf{T} - (\nabla\mathbf{u} \cdot \mathbf{T})^\dagger + \xi[\mathbf{D} \cdot \mathbf{T} + (\mathbf{D} \cdot \mathbf{T})^\dagger]\}^{n+1/2};$$

stage 2

$$\nabla^2(p^{n+1} - p^n) = \frac{2}{\Delta t}\nabla \cdot \mathbf{u}^*;$$

stage 3

$$\frac{2}{\Delta t}(\mathbf{u}^{n+1} - \mathbf{u}^*) = -\nabla(p^{n+1} - p^n).$$

The many aspects of this formulation are now apparent. The predictor step to time level $t^{n+1/2}$ at stage 1a determines the solution increment in both velocity and stress subject to pressure gradient terms at t^n. The corrector step at stage 1b generates an intermediate solution subject to this predicted half-time step solution. The Poisson equation at stage 2 computes the temporal increment in the pressure field as a consequence of the non-solenoidal $\mathbf{u}^*$-field. At stage 3 the temporal shift in the pressure field then finally determines the increment in the solenoidal velocity field $(\mathbf{u}^{n+1} - \mathbf{u}^*)$. A Crank–Nicolson splitting of the pressure terms across the equation stages ensures second-order accuracy; consistent with this, a similar splitting within the momentum equations for the viscous diffusion terms introduces a semi-implicit time-stepping procedure. Such a fractional staged-approach provides dual benefits of rendering large systems computationally tractable and may solve accurately viscous incompressible flows that display mixed type in the underlying partial differential equations.

We adopt a finite element spatial discretization to complete the formulation. Based on the Galerkin weighted residual approach, we introduce approximations $U(\mathbf{x}, t)$, $T(\mathbf{x}, t)$ and $P(\mathbf{x}, t)$ to the velocity, stress and pressure fields respectively over finite-dimensional function spaces:

$$U(\mathbf{x}, t) = U^j(t)\phi_j(\mathbf{x}), \qquad T(\mathbf{x}, t) = T^j(t)\phi_j(\mathbf{x}), \qquad P(\mathbf{x}, t) = P^j(t)\psi_j(\mathbf{x}),$$

where $U(t)$, $T(t)$ and $P(t)$ are nodal values of velocity, stress and pressure respectively, and ϕ and ψ are their respective piecewise continuous shape functions (same forms apply to $\mathbf{u}^*$). The ϕ_j are selected as quadratic functions over six-noded triangular elements, while the ψ_j are linear functions

defined on vertex nodes. Substituting these expressions into the three-staged equations of the solution algorithm and adopting a generalized Galerkin weighted residual approach, a set of discretized equations is obtained as described in Reference 11.

For highly convective flows we have found it appropriate to introduce a consistent streamline spatial weighting for the constitutive equations. This approach is explored and detailed by Carew *et al.*[10] Owing to the nature of the present problems, being both highly elastic and convection-dominated through the stress equation, we find it necessary to employ such a strategy to suppress streamwise numerical diffusion. Other mechanisms are invoked to account for numerical discretization error that takes effect normally to the flow direction.

In a structured approach to the analysis of these strongly extensional flows, where side boundary conditions may be free from constraint, we find it instructive to initially address these test problems with frozen kinematic fields. This implies adopting analytic velocity and pressure fields for the sink flow problem and Newtonian computed fields for the model draw-down problem. Such a frozen coefficient approach was documented in Reference 11 and serves its purpose as a first step prior to solving the fully coupled problem, commencing from this localized solution on the evolutionary search for a steady state.

Once an algebraic system is derived, a combination of iterative and direct solvers is employed to compute the solution increment nodal vectors at each fractional equation stage on every time step. A choice of Jacobi iteration with row-sum diagonal preconditioning is found to be most suitable for all stages, with the exception of stage 2. A small number of iterations and an element-by-element strategy yield a powerful and efficient procedure. A Choleski direct method is utilized at stage 2 for the sparse banded symmetric subsystem that results. A practical choice of time step on the grounds of accuracy and stability is found to be $\Delta t = 0{\cdot}01$ for sink flow and model draw-down for the meshes employed, and $\Delta t = 0{\cdot}001$ for conical section draw-down. The details on such solvers and their implementation are discussed elsewhere.[12,13]

SINK FLOW

The schematic representation of sink flow is shown in Figure 2(a). This represents radial sink flow from the outer radius $r = R_0$ to the inner radius $r = R_i$ with radial velocity component given by $u = -k/r$ and the plane of z normal to the flow. All remaining velocity components vanish.

The dominant stress in this flow is the normal radial extra-stress T_{rr}. For an Oldroyd-B model the elastic normal radial extra-stress is given by the analytic form[14]

$$T_{rr} = \frac{2\mu_1 k}{r^2} + \frac{C_r}{r^2}\exp\left(\frac{r^2}{2\lambda k}\right), \tag{7}$$

where C_r is a constant of integration. Non-dimensionally, imposing a boundary condition $T_{rr} = \sigma$ on $r = R_0$ yields

$$T_{rr} = \frac{2\mu_1 k}{r^2}\left[1 - \left(\frac{R_0^2\sigma}{2\mu_1 k} - 1\right)\exp\left(\frac{1}{2Wek}(r^2 - R_0^2)\right)\right]. \tag{8}$$

To serve as a useful model problem, we solve the sink flow numerically in two dimensions in the r–z plane (see Figure 2(b)) with the fixed kinematics given above. In this analysis we have chosen to imposed relaxed stress at the inlet ($r = R_0$), for which we take σ to vanish in the viscoelastic case. The $z =$ constant boundary surfaces are zero-traction surfaces devoid of shearing. Here we may choose to treat the surfaces as free from constraint or impose analytic stress values.

The parameters chosen for this flow are $R_0 = 2$, $R_i = 1$ and $k = 2$, implying an initial velocity $u = -1$ (at R_0) and a final velocity $u = -2$ (at R_i). The axial co-ordinates are taken as $z_0 = 0$ and $z_L = 1$. The viscoelastic constitutive model is that of Oldroyd-B,[15] which is a specific form of the Phan-Thien/Tanner model with $\varepsilon = 0$ and $\xi = 0$, the other parameters being taken as $\mu_1 = 0{\cdot}8888$, $\mu_2 = 0{\cdot}1112$ and relaxation time $\lambda = 1$. For this flow we take non-dimensional values of Reynolds and Weissenberg numbers as $Re = 1$ and $We = 1$ respectively.

To analyse stress growth with increasing relaxation time, we also solve this problem for $We = 5$, 10, 15 and 20. The solutions for increasing Weissenberg number ($We^{(0)} = 1, \ldots, We^{(4)} = 20$) are determined through a continuation procedure. Steady state solutions for $We^{(i)}$ are determined using the solution for $We^{(i-1)}$ as the initial stress field; for $We^{(0)}$ the stresses are initially relaxed. The problems are solved on a rectangular domain with a finite element mesh in the $r-z$ plane, consisting of 10 subdivisions radially and five axially. This provides a rectangular tessellation upon which each rectangle is subdivided into a pair of triangular finite elements.

In Figure 3 we show the temporal development of the elastic normal extra-stress T_{rr} as a field plot on the flow domain for $We = 1$ and mass iteration number $mitn = 1$ (see below for more detail). The times shown are in dimensionless units; the solution for $t = 52$ represents the steady state solution. The solution oscillates in the axial direction during its temporal development, with oscillations that decay and vanish as a steady state is approached. In Figure 4, T_{rr} is plotted in the radial direction at the fixed axial position $z = 0{\cdot}4$. We observe that there are no radial oscillations in the developing solution and that the analytic solution is satisfactorily achieved by a time $t = 52$ units.

Whilst cross-stream oscillations in the developing solution are suppressed in this case via the time-stepping procedure, this may not be true for more complex problems. Here a unique opportunity is presented to isolate cross- stream oscillations and analyse their numerical dependences. To this end we seek to understand why these oscillations occur and offer methods to overcome their

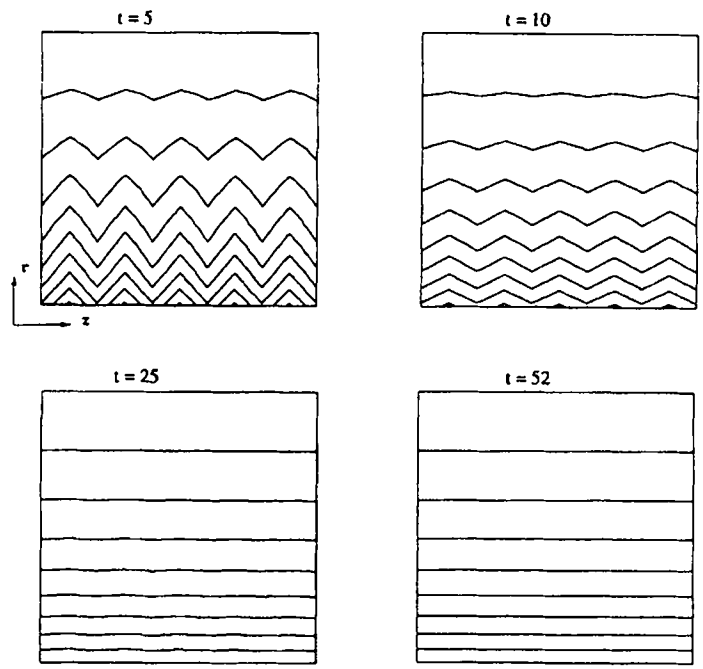

Figure 3. Developing T_{rr} profiles for sink flow; $We = 1$, $mitn = 1$

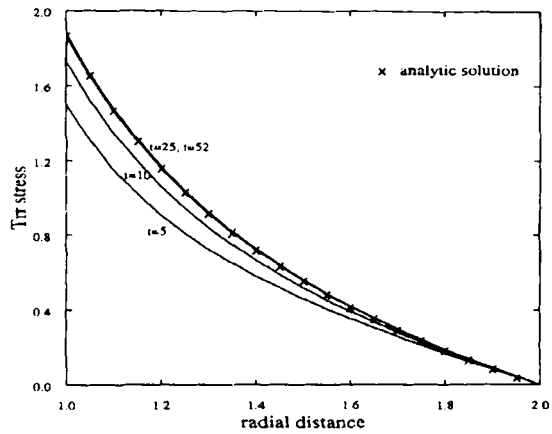

Figure 4. Developing T_{rr} radially for sink flow at axial position $z = 0{\cdot}4$; $We = 1$, $mitn = 1$

development. By fixing values of stress on traction-free side boundaries, we force the problem to become more aware of its one-dimensional nature. Figure 5 shows the solution at time $t = 5$ for the problem where stresses are allowed to find their own level, compared with the instance where stresses are fixed on side boundaries. We note that imposing stresses assists in reducing the width of cross-stream oscillations, though they remain clearly visible in the core flow.

Within the flow solver at each time step a Jacobi iteration is invoked on three separate equation stages. Each stage is governed by a mass matrix and a number of Jacobi iteration domain sweeps are performed to solve the associated equation. Diagonal preconditioning is found to be appropriate on row sums and only a handful of sweeps are deemed necessary. We may choose one iteration sweep (which renders mass lumping), or correspondingly three, five or seven iterations,[13] to test the effect on accuracy of the various iteration numbers. A larger iteration number (*mitn*) implies a more accurate solution on each particular time step, but at greater cost. For the results reported so far we have used a mass iteration number of unity ($mitn = 1$). Figure 6 shows the temporally developing solution for T_{rr} at time $t = 5$ for iteration numbers of one, three, five and seven. By increasing the number of iterations, the cross-stream oscillations are eliminated and a steady state is rapidly reached

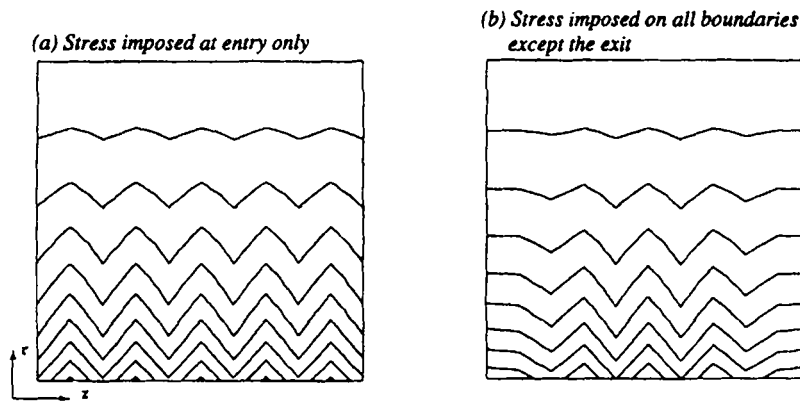

Figure 5. T_{rr} profiles at time $t = 5$ for sink flow; $mitn = 1$, $We = 1$; traction boundary conditions (a) free and (b) fixed

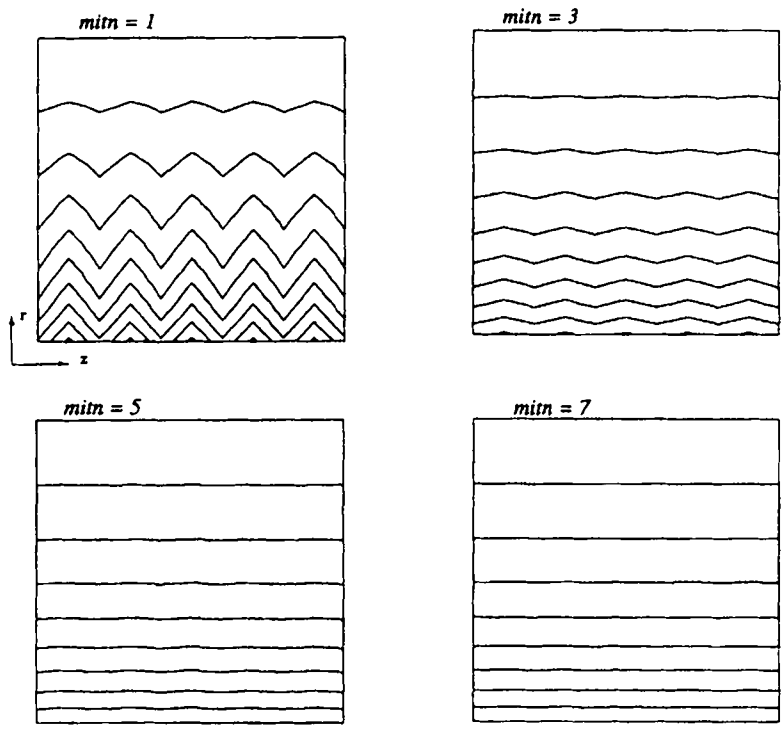

Figure 6. T_{rr} profiles at time $t = 5$ for sink flow; $We = 1$, $mitn = 1$, 3, 5 and 7

with iteration numbers of five and seven. In Figure 7, T_{rr} is plotted in the radial direction at the fixed axial position $z = 0{\cdot}4$; damping out oscillations necessitates fewer time steps to reach the analytic solution. This is gathered by inspection of Figures 7 and 4. The implication here is that although more cost penalty is incurred at larger iteration numbers, overall the cost is equivalent to the single-iteration alternative. Furthermore, we have identified that accuracy on each iteration step is a vital factor in removing cross-stream oscillations.

The oscillations described are present owing to differences in the developing solution at vertex and mid-side nodes of the triangular finite elements of the mesh. We investigate another method that may also prove effective in eliminating oscillations in the temporally-developing solution: smoothing the stress normal to the flow (streamline upwinding is employed to smooth oscillations in the flow direction). We may achieve this by linear interpolation: for each mid-side node of a triangular finite element we can take an averaged value of stress dependent on the values at its two shared vertex nodes at each time step. Averaging for the mid-side node at an angle to the principal direction of flow is based on the four vertex nodes of triangular finite element pairs. This overcomes errors introduced by interpolation over the spatial triangulation. Although stress smoothing may remove oscillations at each time step, the ultimate requirement is to achieve the same through the overall time-stepping solution process. The result of stress smoothing for sink flow is shown in Figure 8 with an iteration number of unity. We observe that the cross-stream oscillations in the developing solution are removed. Nevertheless, we note two points. First, stress smoothing has introduced a distortion into the stress field (compare with the plot for $t = 52$ in Figure 3). Second, the maximum value of the elastic normal extra-stress T_{rr} increases far in excess of the steady state maximum value of 1·8758; this continues to grow and ultimately leads to numerical divergence in the time-stepping procedure.

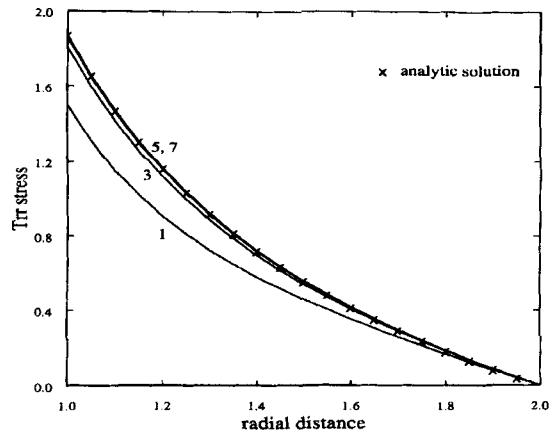

Figure 7. T_{rr} radially for sink flow at time $t=5$ at axial position $z=0{\cdot}4$; $We=1$, $mitn=1$, 3, 5 and 7

Such behaviour is demonstrated graphically in Figure 9, with T_{rr} plotted in the radial direction at the fixed axial position $z=0{\cdot}4$. Similar behaviour is observed for stress smoothing if we increase the number of mass iterations to seven, whereupon the numerical scheme diverges in fewer time steps.

The steady state T_{rr} stress profiles in the radial direction for values of We up to 20 are shown in Figure 10. We have employed seven mass iterations in determining these results. Also shown in this plot are the corresponding analytic stresses given by expression (8). We recall that increasing the Weissenberg number is directly related to increasing the relaxation time of the fluid. We can see that the computed solutions compare favourably with the analytic stress profiles. Increasing We leads to a decrease in the level of stress, as the fluid experiences the same extension from an initial stress-free

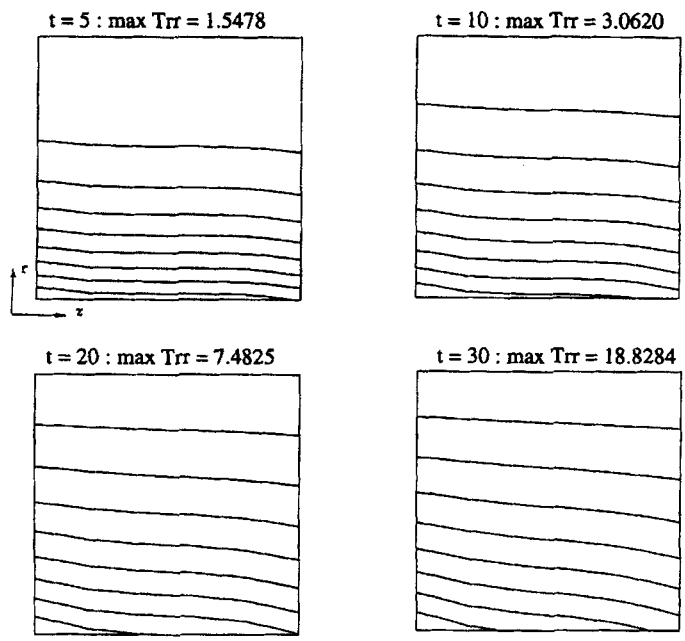

Figure 8. Developing T_{rr} profiles for sink flow with stress smoothing normally and tangentially; $We=1$, $mitn=1$

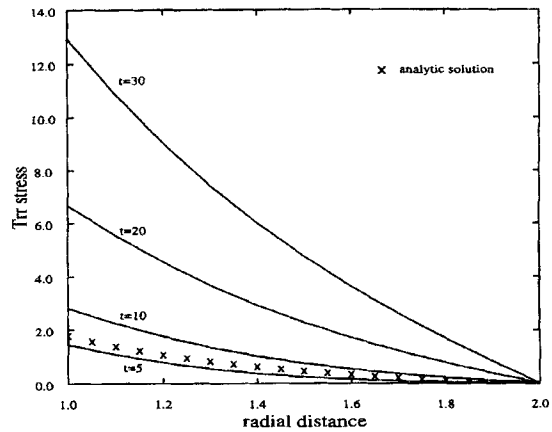

Figure 9. Developing T_{rr} radially for sink flow at axial position $z = 0{\cdot}4$ with stress smoothing normally and tangentially; $W = 1$, $mitn = 1$

state. Also in Figure 10, stress plots are displayed using the analytic expression (8), assuming a fixed time scale of operation. The full curve represents a viscous response implying a relaxed stress at infinity that is independent of We, since $R_0^2\sigma/(2\mu_1 k) - 1 = 0$. By fixing the stress as zero at the radial distance 2·0 and increasing the relaxation time of the material, we observe greater elastic behaviour. For a fixed time scale, increasing the relaxation time of the material has the effect of delaying stress growth from an initial stress-free state. One may also observe from (8) that stress growth with increasing We will arise dependent on the choice of inlet boundary value σ.

For the steady state solutions reported thus far we have employed a decoupled solution approach, whereby the viscoelastic stresses are determined on the basis of frozen kinematics. This allows for simpler computations and the isolation of numerical dependences that may arise in the solution of the viscoelastic constitutive equation. If the decoupled approach is successful, it is then desirable to commence from the decoupled solution as the initial field data for the corresponding coupled problem. By solving the governing equations as a coupled system, we solve for velocity, pressure and

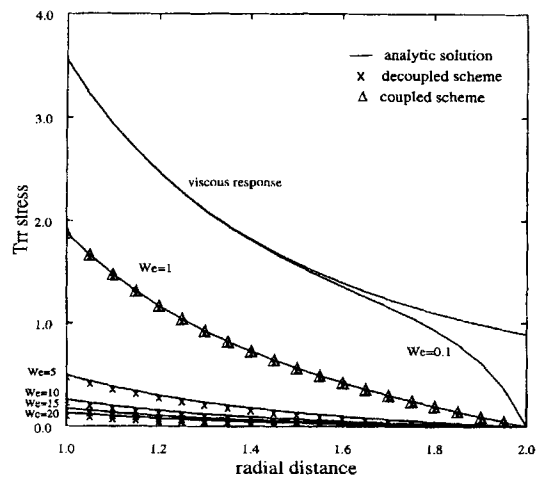

Figure 10. Steady state T_{rr} for sink flow; $We = 1$, 5, 10, 15 and 20; comparison with analytic solution

stresses that are consistent with the viscoelastic flow. In this manner we have determined a steady state solution for $We = 1$ using the coupled approach with a mass iteration number of seven. The steady state solution for T_{rr} plotted radially is also displayed in Figure 10 for direct comparison against the decoupled solution. In this instance the two solution schemes give essentially identical results owing to the fact that the velocity field is largely unaffected by the viscoelastic stresses.

MODEL DRAW-DOWN

The geometry of the model draw-down problem is shown in Figure 2(c). The fluid enters the geometry with a resultant velocity of magnitude W_0 and exits at a resultant velocity of magnitude W_L. The direction in which the velocity acts at any radial position is determined by the angle formed relative to the position of the intersection of the projected traction-free surface and the axis of symmetry. The inlet and outlet velocities are related through the flow rate Q. The average cross-sectional resultant velocity $W = Q/\pi R^2$, so that the draw-down ratio is given by

$$D_R = \left(\frac{R_0}{R_L}\right)^2 = \frac{W_L}{W_0}, \tag{9}$$

where R_0 and R_L are the initial and final radii respectively.

Along the traction-free surface the velocity is taken as the resultant velocity which is approximated again from the condition of constant flow rate. Hence $W = Q/\pi R^2$, where R is a linear function of axial position. The radial and axial velocities can then be recovered from the transformation $u = -W \sin\theta$ and $w = W \cos\theta$, where θ is the angle of inclination of the traction-free surface. The dominant stress in this flow is the normal axial extra-stress T_{zz}. The stress is relaxed at the inlet; also, the shear stress vanishes on the axis of symmetry, since this represents a shear-free boundary. The growth of stress is monitored at various times in the establishment of a steady state solution.

The geometrical parameters for the problem are $R_0 = 1$, $R_L = 1/\sqrt{2}$ and $L = 10$, where the angle of inclination of the free surface is $\theta \approx 2°$. The inlet velocity is taken as $W_0 = 1$ and the draw-down ratio as $D_R = 2$, so $W_L = 2$. The viscoelastic model selected for this problem is the exponential version of the Phan-Thien/Tanner model, as described earlier, with model parameters $\mu_1 = 0{\cdot}8888$, $\mu_2 = 0{\cdot}1112$, $\lambda = 1$, $\varepsilon = 0{\cdot}1$ and $\xi = 0{\cdot}01$, with $Re = 1$ and $We = 1$. The model possesses the material behaviour of extension- and shear-thinning viscosities. The choice of model, ε and ξ reflects viscometric behaviour consistent with that exhibited by molten polyethylenes, as described in Reference 7.

To analyse the influence on the numerical solution of a change in mesh, the problem is solved on four finite element meshes (meshes 1–4; see Figure 11(a)), with mesh refinement in the z-direction (meshes 1–3) and refinement in the r-direction (meshes 2 and 4). For each mesh we determine the velocity field for an equivalent Newtonian flow and compute viscoelastic stresses based on this frozen kinematic field. We also consider flow for higher Weissenberg numbers $We = 5$, 10, 15 and 20, employing a continuation procedure as above. For these analyses we use mesh 2 of Figure 11(a). Solutions are also determined using a coupled approach.

To begin, we employ one mass iteration ($mitn = 1$) in our computations for the model draw-down problem. The velocity field for one of the meshes (mesh 4: 5×60) is shown as a vector plot for resultant velocity in Figure 11(b). We observe the plug-like nature of the flow with velocity increasing from the inlet to the outlet.

Figures 12(a)–12(c) show the temporal development of T_{zz} along the axis of symmetry for meshes 1–3 respectively at $We = 1$ (the times shown are again in dimensionless units). We observe that the solution shows axial oscillations in its early temporal development on each mesh and that these

(a)

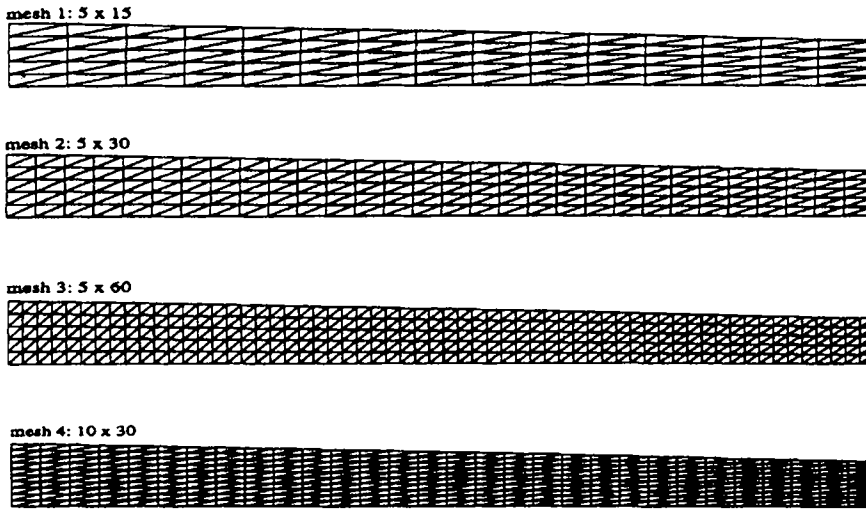

(b)

Figure 11. Model draw-down: (a) finite element meshes; (b) resultant velocity field on 5 × 60 mesh

oscillations are damped out as a steady state is approached (the upper curve for each mesh). Increasing the number of elements in the axial direction serves to reduce the amplitude of the oscillations in the solution in the early stages of development and ultimately the solutions on all three meshes are in agreement.

Figures 12(d) and 12(e) show the development of T_{zz} radially at axial position $z = L/2$ for meshes 2 and 4 respectively at $We = 1$. We again see oscillations in the developing solution and note that here increasing the number of elements in the radial direction serves only to increase the frequency of the oscillations and has no effect on their amplitude. Ultimately these oscillations are damped out through the time-stepping procedure and a steady state solution is reached (the straight lines in these plots). Also shown in Figure 12(d) and 12(e) is a bias in the developing solution at the traction-free boundary (radial distance 0·8) compared with that at the axis of symmetry (radial distance 0·0). This biasing was not present in sink flow (see Figure 3, for example) and is due to the fact that the radial distance vanishes at the axis for the model draw-down problem, the small size of r thus having an

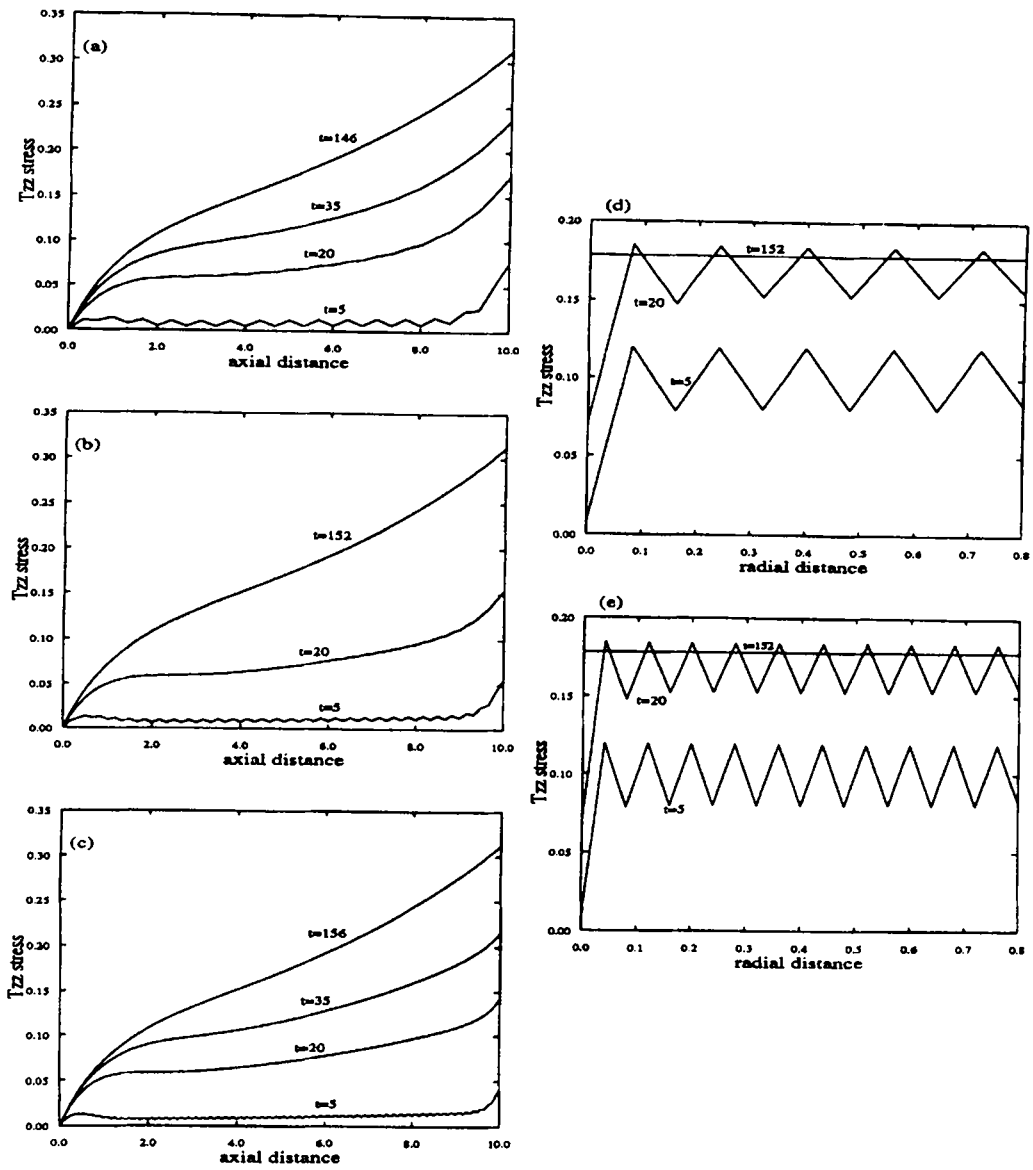

Figure 12. Model draw-down: (left) developing T_{zz} along axis of symmetry on (a) 5 × 15 mesh, (b) 5 × 30 mesh and (c) 5 × 60 mesh; (right) developing T_{zz} radially at axial position $z = L/2$ on (d) 5 × 30 mesh and (e) 10 × 30 mesh; $We = 1$, $mitn = 1$

effect on the determination of the solution at each time step. Allowing the shear stress to be determined at the axis of symmetry instead of being imposed, as previously, has no effect on this biasing. In the steady solution the normal stresses dominate the shear stress and reflect radially constant profiles.

To further interrogate the source of these numerical oscillations and investigate their removal, we again turn to increasing the accuracy of the algorithm on each time step by employing a strategy that proved successful for sink flow. To test the effect of increasing the number of mass iterations per time

step on the evolution to a steady state, we illustrate in Figure 13 the temporal development of T_{zz} to steady state both axially ((a) and (b)) and normally ((c) and (d)), for a mass iteration number of seven compared with the results for a mass iteration number of unity. Increasing the number of mass iterations reduces the amplitude of the oscillations in the developing solution, as observed for sink flow. By employing a mass iteration number of seven, we also reduce the number of time steps required to reach the steady state (compare $t = 146$ as the time to reach a steady state for a mass iteration number of unity with $t = 28$ for a mass iteration number of seven). The cost of each alternative approach is again comparable, though clearly superior accuracy is achieved for the higher iteration number.

The steady state T_{zz} stress profiles along the axis of symmetry for values of *We* up to 20 are shown in Figure 14(a). A mass iteration number of seven was used in each case. As for sink flow, the increase in *We* has the effect of delaying stress growth, as the fluid experiences the same extension from a stress-free state. The plot for $We = 1$ shows a qualitative difference from plots at higher values of *We*: the stress gradient is much greater in its early spatial development. A similar feature is evident for Figure 10 at $We = 0{\cdot}1$ and may be attributed to a greater viscous response.

For this problem we have determined steady state solutions through a coupled approach, as above, at Weissenberg numbers $We = 1$ and 10 with a mass iteration number of seven. Plots for T_{zz} along the axis of symmetry for both schemes at each value of *We* are also shown in Figure 14(a). We again see that the two solution schemes give essentially identical results, since the velocity field is largely unaffected by the viscoelastic stresses. Hence interaction between the velocity and stress fields does

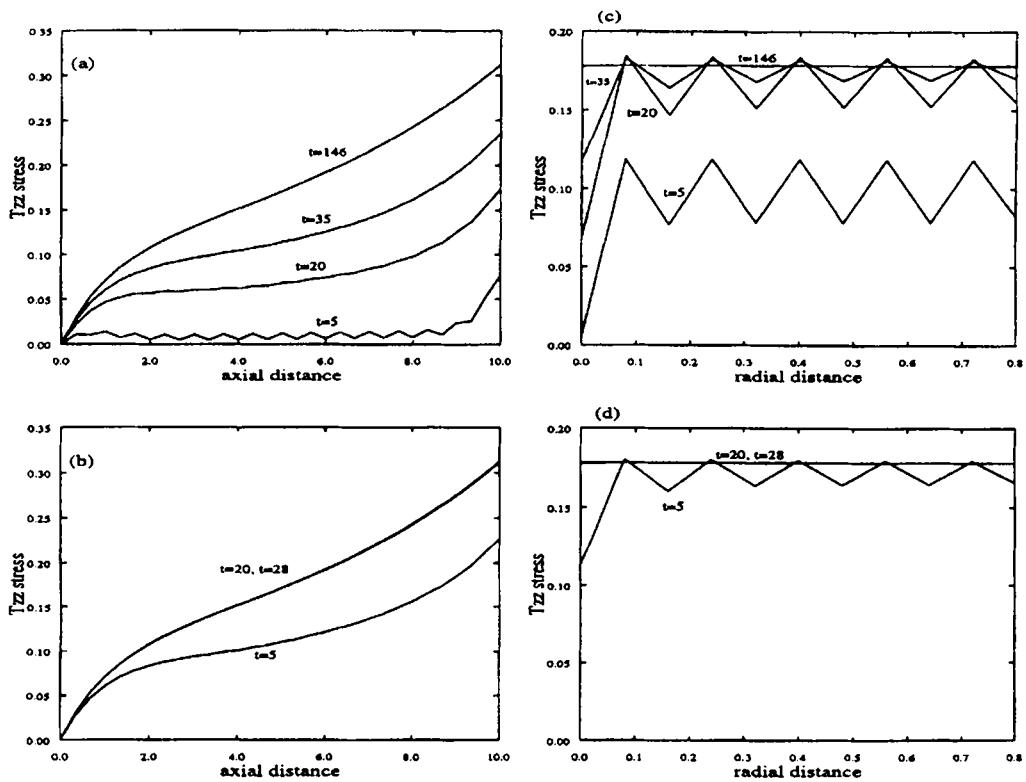

Figure 13. Model draw-down on 5 × 15 mesh: (left) developing T_{zz} along axis of symmetry with (a) *mitn* = 1 and (b) *mitn* = 7; (right) developing T_{zz} radially at axial position $z = L/2$ with (c) *mitn* = 1 and (d) *mitn* = 7; $We = 1$

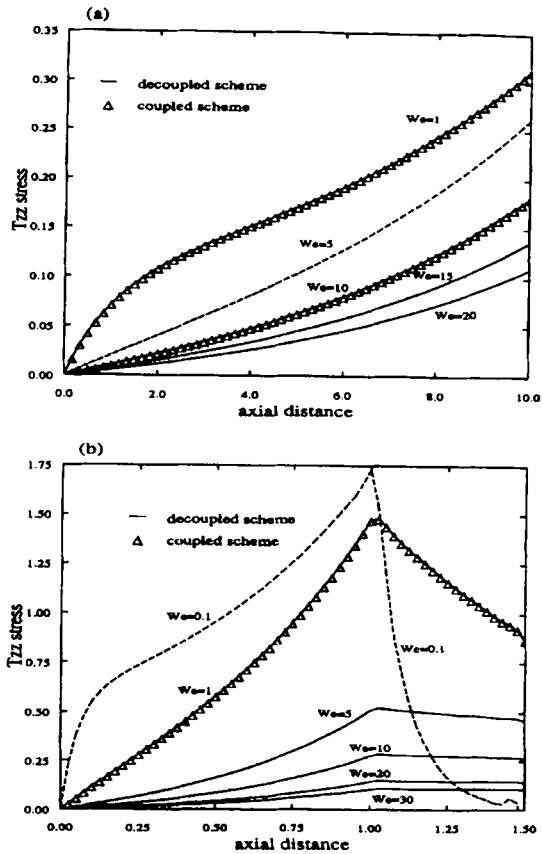

Figure 14. (a) Steady state T_{zz} along axis of symmetry for model draw-down; $We = 1$, 5, 10, 15 and 20, $mitn = 7$. (b) Steady state T_{zz} along streamline for conical section draw-down; $We = 0{\cdot}1$, 1, 5, 10, 20 and 30, $mitn = 7$

not pose any new complications under these conditions. Here we are assuming that the location of the traction-free surface is fixed (a slip boundary), that the net flux across this boundary vanishes and accordingly we have taken frozen resultant velocities there.

CONICAL SECTION DRAW-DOWN

A schematic illustration of the conical section draw-down geometry is shown in Figure 2(d). For the previous model problems we have modelled only stress growth. We now consider stress growth in the extension region, caused by the pulling action of the moving boundary, and the subsequent stress relaxation as the fluid travels in contact with this boundary.

Along the traction-free surfaces the velocity is taken as the resultant velocity approximated from the condition of constant flow rate, in a similar manner as described for model draw-down. The draw-down ratio for this flow is given by (see Figure 2(d))

$$D_R = \frac{R_0^2 - R_i^2}{R_t^2 - R_c^2} = \frac{W_c}{W_0}, \tag{10}$$

where R_0 and R_i are the outer and inner radii of the tube tooling exit respectively, and R_t and R_b are the coating and cable radii respectively. The velocity W_c is the cable velocity and W_0 is the resultant velocity at the inlet. The dominant stress in this flow is the normal axial extra-stress T_{zz}. The stress is assumed to be relaxed at the inlet. As discussed and observed for the two previous model problems, we would expect the stress growth to be dictated by the relaxation time of the material. Furthermore, for this study we can analyse the effect of relaxation time on stress relaxation.

The geometric parameters for the problem are such that the draw-down ratio is two, the angle of inclination of the outer traction-free surface is about 4° and the inner traction-free surface is at an angle of about 3°. The viscoelastic model selected is again the exponential version of the Phan-Thien/Tanner model, with parameters chosen to reflect the shear- and extension-thinning nature and first normal stress difference behaviour of low- density polyethylene.[7] The model parameters are

$$\mu_1' = \mu_1/\mu_0 = 0{\cdot}9995, \qquad \mu_2' = \mu_2/\mu_0 = 0{\cdot}0005, \qquad \lambda = 5 \text{ s}, \qquad \varepsilon = 0{\cdot}1, \qquad \xi = 0{\cdot}01,$$

where $\mu_0 = \mu_1 + \mu_2$ is the zero-shear viscosity. The characteristic length is taken to be the draw-down length and the characteristic velocity is taken to be the velocity of the moving boundary. The Reynolds and Weissenberg numbers for this flow are taken as $Re = 2{\cdot}78 \times 10^{-4}$ and $We = 30$. As discussed earlier, we employ a continuation procedure to attain steady state solutions up to this value of Weissenberg number.

These problems are solved on a regular mesh of five subdivisions radially and 30 subdivisions axially. The viscoelastic stresses for each value of We are determined based on the frozen kinematic field for an equivalent Newtonian flow and seven mass iterations are employed.

The resultant velocity along an internal streamline gradually increases with axial distance, rising from a value of half at inlet to unity on meeting the moving boundary (axial distance 1·0), and subsequently remains at this unitary level. At the geometry exit we have imposed an outlet axial velocity of unity, which generates a small discrepancy between the numerical and the imposed velocity field. This problem can be remedied by computing the exit boundary velocity values.

The steady state T_{zz} stress profiles along a streamline in the flow for values of Weissenberg number from 0·1 to 30 are provided in Figure 14(b). We again see similar behaviour for stress growth to that observed for the prior model problems. A further point to discuss here is the stress relaxation, which occurs in the flow section after the fluid meets the moving boundary. The relaxation of stress in this region is shown to be dependent on the relaxation time for a fixed process time scale. The elevation of stress level is itself governed by the inflow stresses, reaching a peak as the polymer meets the moving boundary and subsequently undergoes relaxation. As anticipated, the decay of stress for the lower value of We ($= 0{\cdot}1$) is much more marked (we recall that for a viscous material the stress would vanish immediately the strain was removed). The slight discrepancy at the exit (axial distance around 1·5) for these stress curves is due to the numerical and imposed velocity adjustment described previously.

It is worth noting that a purely viscous material would exhibit an initial non-zero extra-stress, since it is dependent on the non-zero velocity gradient at the geometry inlet. The next step is to impose a realistic stress level at inlet and investigate the subsequent stress growth for viscoelastic flow. This leads us naturally to analyse the predominantly shearing flow in the tube tooling geometry and thus provide the inflow stress field for the draw-down section.

The above results are derived according to a decoupled analysis. Finally we have invoked a coupled solution approach for this problem at $We = 1$, as described earlier. The resulting stress profiles, as shown in Figure 14(b), prove to be practically identical with those for the decoupled scheme, in keeping with our earlier findings. Consistency in all solutions reported is concluded.

CONCLUSIONS AND DISCUSSION

Studying model problems relevant to wirecoating has given an insight into the difficulties that may arise in determining stress fields for convection- dominated viscoelastic flows. Sink flow is a one-dimensional convection problem for stress, representing the dominant flow behaviour of draw-down and possessing an analytic solution. By solving this flow in two dimensions, we have been able to investigate various aspects of the numerical solution procedure in the isolation of extensional flow and consider their effect on the temporal development of the viscoelastic stresses. Model draw-down represents a slightly more complex problem in that radial variation along the axial direction is introduced through an inclined traction-free surface, generating a two-dimensional flow with some shear. For these problems, oscillations (streamwise for model draw-down and cross-stream for both) are observed in the temporally developing solution for the viscoelastic stresses. These oscillations are ultimately suppressed in both cases through the time-stepping procedure. Finally, for conical section draw-down we have applied the knowledge gathered in the first two model problems to more realistic processing conditions. This more complex problem illustrates the effects of stress growth through extensional flow in combination with stress relaxation as the coating polymer travels in strain-free flow in contact with the moving boundary.

The key findings of this study are applicable not only to the problems in hand but also to more complex convection-dominated flows that manifest sufficiently severe oscillations. Specifically, to attain accurate solutions, mesh refinement streamwise with streamline upwinding may control oscillations in that direction, whilst enhancing localized accuracy through increasing the number of Jacobi iterations may suppress cross-stream oscillations. We have demonstrated that these strategies can be effective in smoothing oscillations in the evolution of the solution. In solving for the stress field for these model problems, we have initially employed frozen kinematics and a decoupled scheme for determination of the stress. We have subsequently determined stresses using a coupled scheme, the results for which indicate little difference in the stress profiles generated between the alternative schemes owing to the nature of the velocity field for these particular problems.

We have solved both sink flow and model draw-down up to $We = 20$ and conical section draw-down up to $We = 30$ to investigate the effect of elasticity on such convection-dominated flows. For the first two problems we have shown that an increasing relaxation time for a fixed process time has the effect of inhibiting stress growth from an initial stress-free state. The maximum stress level attained is shown to decrease with increasing We. This holds for conical section draw-down in the extension region up to the moving boundary. In the relaxation region of the flow domain, where the fluid travels in contact with the moving boundary, stress is allowed to relax and an increasing value of We has the effect of inhibiting stress decay. The implication is that for larger values of We, longer times will be required for the stress to decay to an acceptable minimal level. This phased study has permitted the gradual consideration of the principal aspects of modelling complexity for tube extrusion.

ACKNOWLEDGEMENTS

Authors wish to acknowledge the financial support of BICC Cables Limited throughout this study and the collaboration with Dr A. R. Blythe and Mr A. A. Mosquera. The authors are grateful for the assistance of Dr I. Mutlu in the final drafting stages of this work.

REFERENCES

1. B. Caswell and R. I. Tanner, *Polym. Eng. Sci.*, **18**, 416 (1978).
2. R. Wagner and E. Mitsoulis, *Adv. Polym. Technol.*, **5**, 305 (1985).
3. E. Mitsoulis, 'Finite element analysis of wirecoating', *Polym. Eng. Sci.*, **26**, 171–181 (1986).

4. J. F. T. Pittman and K. Rashid, 'Numerical analysis of high-speed wirecoating', *Plast. Rub. Proc. Appl.*, **6**, 153 (1986).
5. E. Mitsoulis, R. Wagner and F. L. Heng, 'Numerical simulation of wire-coating low-density polyethylene: theory and experiments', *Polym. Eng. Sci.*, **28**, 291–310 (1988).
6. A. R. Blythe, S. Gunter, A. A. Mosquera, P. Townsend and M. F. Webster, 'Modelling polymer melt flows in wirecoating processes', *J. Non-Newtonian Fluid Mech.*, May 1996, 16 pp; also available as *Comput. Sci. Rep. 17-95*, Department of Computer Science, University of Wales, Swansea, 1995.
7. K. Walters, D. M. Binding and R. E. Evans, 'Modelling the rheometric behaviour of 3 polyethylene melts', *Tech. Rep.*, Institute of Non- Newtonian Fluid Mechanics, University of Wales, Aberystwyth, 1994.
8. H. M. Laun and H. Schuch, 'Transient elongational viscosities and drawability of polymer melts', *J. Rheol.*, **33**, 119–175 (1989).
9. N. Phan-Thien and R. I. Tanner, 'A new constitutive equation derived from network theory', *J. Non-Newtonian Fluid Mech.*, **2**, 353– 365 (1977).
10. E. O. A. Carew, P. Townsend and M. F. Webster, 'A Taylor–Petrov– Galerkin algorithm for viscoelastic flow', *J. Non-Newtonian Fluid Mech.*, **50**, 253–287 (1993).
11. E. O. A. Carew, P. Townsend and M. F. Webster, 'Taylor–Galerkin algorithms for viscoelastic flow: application to a model problem', *J. Numer. Methods PDE*, **10**, 171–190 (1994).
12. D. M. Hawken, H. R. Tamaddon-Jahromi, P. Townsend and M. F. Webster, 'A Taylor–Galerkin based algorithm for viscous incompressible flow', *Int. j. numer. methods fluids*, **10**, 327–351 (1990).
13. D. Ding, P. Townsend and M. F. Webster, 'The iteration solution of Taylor–Galerkin augmented mass martix equations', *Int. j. numer. methods eng.*, **35**, 241–253 (1992).
14. R. I. Tanner, *Engineering Rheology*, Clarendon, Oxford, 1985.
15. J. G. Oldroyd, 'On the formulation of rheological equations of state', *Proc. R. Soc. Lond. A*, **200**, 523–541 (1950).